Clays and Clay Minerals, Vol. 65, No. 2, 104–121, 2017.

CHARACTERIZATION OF THE SECOND PACKAGE OF THE ALTERNATIVE BUFFER MATERIAL (ABM) EXPERIMENT – II EXCHANGEABLE CATION POPULATION REARRANGEMENT

R. Dohrmann[1,2,*] and S. Kaufhold[1]

[1] Bundesanstalt für Geowissenschaften und Rohstoffe (BGR), Stilleweg 2, D-30655 Hannover, Germany
[2] Landesamt für Bergbau, Energie und Geologie (LBEG), Stilleweg 2, D-30655 Hannover, Germany

Abstract—Bentonites are candidate materials for encapsulating radioactive waste within barrier systems in crystalline rocks. In the 'Alternative Buffer Material' (ABM) test in the hard rock laboratory in Äspö, Sweden, six packages of eleven different buffer materials (mainly bentonites) with various exchangeable cation populations were packed vertically with an iron tube used as a heater in the center. After installation, the second 'ABM package' (ABM-II) was first allowed to saturate with water for approximately 2.5 years. The blocks were then exposed to a temperature of up to 141ºC for approximately 3–4 years. The hypotheses for the present study were: (1) no horizontal gradient of the cation exchange population was present in the individual blocks of ABM-II because ABM-II had a longer reaction time in comparison to the ABM-I package, which did not have horizontal gradients; (2) the exchangeable cation Ca^{2+}:Na^{+}:Mg^{2+} ratio was equal in all blocks of ABM-II and was independent of block position in the package. As expected from ABM-I, all blocks in the ABM-II experiment showed large differences between the measured values of the reference materials and the reacted samples. The exchangeable Na^{+} and Mg^{2+} values in ABM-II were reduced by up to 55% to 59% in comparison to the reference material. Contrary to the first hypothesis, horizontal gradients were observed in ABM-II; and, contrary to the second hypothesis, the exchangeable cation ratios differed markedly in the different reacted buffer materials. The largest total Na^{+} loss was observed in the middle part (–67%), whereas Mg^{2+} values decreased by 79% in the upper part. The exchangeable Ca^{2+} values increased strongly in ABM-II, particularly in the upper part. The most useful parameter to distinguish between ion exchange equilibria of ABM-I and ABM-II was the Na^{+}/Mg^{2+} ratio. This ratio was constant in ABM-I (3.0) and had a similar ratio (3.5) in the lower part of ABM-II; however, the ratio strongly increased (5–10) in the upper part of the ABM-II package. The large Na^{+}/Mg^{2+} ratios in the upper part of ABM-II could possibly be explained by water loss into the rock (caused by a pressure drop and boiling) and subsequent water uptake.

Key Words—Bentonite Buffer, Boiling, CEC, Cu-trien5xcalcite, Exchangeable Cation Population.

INTRODUCTION

Bentonites are candidate materials for the encapsulation of High Level Radioactive Waste (HLRW), but much work is yet needed to understand more completely the long-term stability of these materials under potential repository conditions. Some concepts for evaluating deep geological storage of HLRW are based on bentonite buffers, which are part of engineered barrier systems (Dohrmann *et al*., 2013a). Under repository conditions, the long term stability of these engineered barrier systems in crystalline rocks as well as in argillaceous rocks depends on the stability of the smectite minerals, particularly with respect to the swelling capacity and the cation exchange capacity (CEC). Details on the use of bentonite as an HLRW barrier material are given by Sellin and Leupin (2014), Kaufhold *et al*. (2017a), Kaufhold and Dohrmann (2016), and van Geet and Dohrmann (2016). Experiments to evaluate the integrity of bentonite barrier systems have been performed on different scales and were discussed by Dohrmann *et al.* (2013b) and others as follows: 1) at the lab scale with the capacity to vary different parameters (*e.g*. Bourg *et al*., 2006; Holmboe *et al*., 2010; Holmboe and Bourg, 2013; Keller *et al*., 2014; Fröhlich, 2015; Elert *et al*., 2015; Wersin *et al*., 2015; Ferrage, 2016; Balmer *et al*., 2017; Grolimund *et al*., 2016; Ishidera *et al*., 2016; Kaufhold *et al*., 2016; Kerisit *et al*., 2016; Klika *et al*., 2016; Peng *et al*., 2016; Rivard *et al*., 2016; Tournassat *et al*., 2016; Kaufhold *et al*., 2017b, 2017c), but such experiments were often far from reality because of the high water:-solid ratios and high temperatures that were used or simply because modelling was performed with no accompanying experiments; 2) field experiments of intermediate size (*e.g*. Plötze *et al*., 2007; Gómez-Espina and Villar, 2016); and 3) full scale experiments performed in hard rock or underground rock laboratories, which have been rarely conducted mainly because of the enormous amounts of materials, preparations, and construction work that is required (Dixon *et al*., 2007; Johannesson *et al*., 2007). Experiments at all scales are necessary to understand the processes related to cation exchange. The most important scale with respect to long-

* E-mail address of corresponding author:
reiner.dohrmann@lbeg.niedersachsen.de
DOI: 10.1346/CCMN.2017.064052

term safety analysis is full scale. Exchangeable cation population ($EC_{population}$) studies are necessary to understand processes in engineered barrier systems that may influence contaminant transport (*e.g.* Mayordomo *et al*., 2016), swelling pressure at low densities, and mechanical strength, etc. (*e.g.* Karnland *et al*., 2006; Kaufhold and Dohrmann, 2016). Bentonite erosion is affected by the amount of exchangeable Na^+ (*e.g.* Kaufhold and Dohrmann, 2008; Missana *et al*., 2011). Physicochemical processes that can affect bentonite erosion, such as the redistribution of exchangeable cations (ECs), therefore, must be understood. Bentonite erosion is of particular interest for such buffer systems. Sellin and Leupin (2014) summarized the research and concluded that future research is needed for "further understanding of the colloid formation/erosion processes – in Sweden and Finland, periods with dilute water after melting of future glaciers cannot be excluded and a large loss of bentonite may have a direct impact on the overall safety of a repository." Variations in the type of bentonite used in HLW disposal concepts was discussed by Kaufhold and Dohrmann (2016). The authors gave an overview about the assessment of parameters to distinguish suitable bentonites from less suitable bentonites and identified ten key issues (*e.g.* low hydraulic conductivity, high self-sealing ability, and durability (stability), compare with Sellin and Leupin, 2014), which were used to discuss bentonite specifications. The Swedish Nuclear Fuel and Waste Management Company (SKB) started an intermediate scale field experiment called the 'Alternative Buffer Material' (ABM) test project (SKB, 2007). In contrast to all former full scale and intermediate scale experiments, more than one type of bentonite was used. The $EC_{population}$ of the buffer materials was initially very different. After the termination of the first ABM-I package experiment, Dohrmann *et al*. (2013b) showed that the $EC_{population}$ had almost completely equilibrated with the surrounding water, which Wallis *et al.* (2016) confirmed by modelling and concluded that the "speed of alterations was linked to high diffusion coefficients under the applied temperatures, which facilitated the propagation of hydrochemical changes into the clays." Among other factors, the diffusive flux is a function of temperature and time. Heat treatments were longer in ABM-II and the longer reaction times were expected to maximize equilibrium of the $EC_{populations}$ between the different buffer materials. The first hypothesis of the present study was that (1) no horizontal gradient of the cation exchange population was present in individual blocks of ABM-II from the rock side to the heater because the ABM-II package has reacted even longer than the ABM-I package, which showed no horizontal gradients. The second hypothesis was that (2) the ratios of the cations Ca^{2+}: Na^+: Mg^{2+} were equal in all blocks of ABM-II and were independent of position in the package because ABM-I was already close to equilibrium as was confirmed by modelling.

The purpose of the present study was, therefore, to study ion exchange reactions in the ABM-II experiment because these reactions proceed much faster in the buffer materials than mineral alteration reactions. The ABM-II experiment differed from ABM-I in the duration of the initial water saturation and the reaction time, which should have had an effect on the $EC_{populations}$.

MATERIALS AND METHODS

ABM design

The setup of the ABM experiment was related to the Swedish KBS-3 concept with a metal canister surrounded by clay situated in crystalline bedrock at approximately 500 m depth (SKB, 2007; Eng *et al.*, 2007). In contrast to the full scale prototype repository *in situ* experiment (PR), which was initiated to study processes in the complete sequence as the processes will occur in repository construction and operation (Johannesson *et al.*, 2007; Dohrmann and Kaufhold, 2014) and the temperature was designed to be above 100ºC in the ABM buffer. The ABM is an intermediate scale experiment (1:4) similar to the 'Long Term Test of Buffer Material' (LOT) *in situ* experiment (Olsson and Karnland, 2011). The main differences between these experiments were that in the LOT experiment only one type of bentonite (MX80) was used and copper instead of common carbon steel (P235TR1) was used for the canister. The reason for not using a copper pipe, as was used in most of the experiments at Äspö HRL, was to be able to study the effects of corroding steel in close contact with the buffer material (Wersin and Birgersson, 2014; Wersin *et al*., 2015; Kaufhold *et al*., 2015, 2017a; Samper *et al*., 2016) and also makes possible the comparison of steel corrosion effects with the copper/bentonite interface (Szakálos and Seetharaman, 2012; Kosec *et al*., 2015; Kaufhold *et al*., 2017b). The ABM experiment was installed in boreholes in the crystalline rock. The bore holes had a diameter of 300 mm and a depth of 3 m. The outer diameter of the ring blocks was 280 mm, the inner diameter was 110 mm, and the height of the individual ring blocks was 100 mm. The outer diameter of the pipe was 108 mm, which was close to the 110 mm inner diameter of the bentonite ring blocks. In each experimental package, three electrical heaters were installed to yield the target temperature in the bentonite blocks. A main heater ran along the entire package length (Figure 1) and two additional heaters were installed. One heater was installed at the bottom and another at the top to compensate for temperature losses at the top and bottom and to give a more homogenous temperature distribution throughout the package. Temperatures varied within the blocks and were approximately 40–50ºC warmer at the bentonite/heater interface than at the bentonite/rock interface. The experiment initially consisted of three packages in three separate boreholes and in 2012 three additional

https://doi.org/10.1346/CCMN.2017.064052 Published online by Cambridge University Press

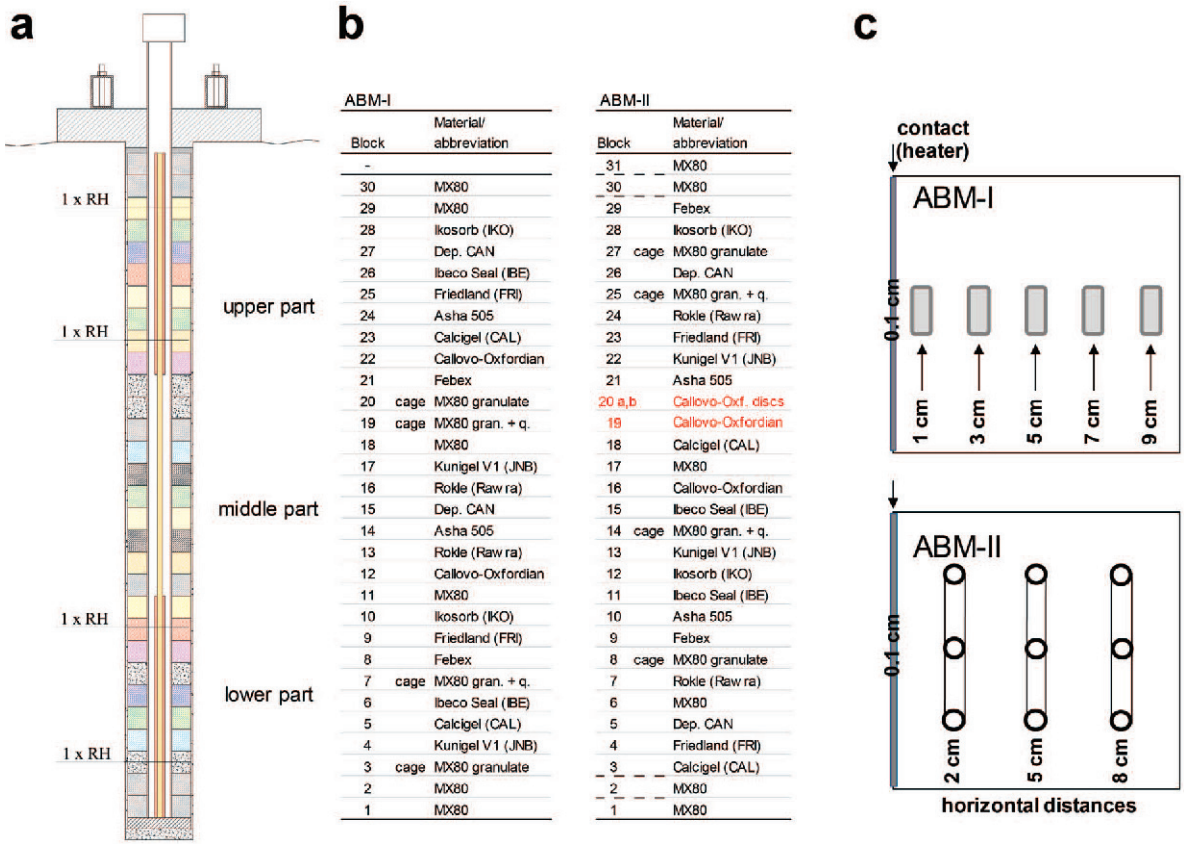

Figure 1. Schematic diagram of the ABM packages showing the positions of (a) the relative humidity (RH) sensors, (b) the block order in the ABM-I and ABM-II (present study) packages, and (c) the sampling schemes. The position designated "Callovo Oxfordian discs" represents two discs of 3–5 cm height each (20a, 20b). Both of the COX blocks at positions 19 and 20 in ABM-II were disintegrated after termination of the experiment and could not be analyzed. The 'MX80 gran + q' = MX80 granulate + quartz and 'cage' indicates the positions of the cages within the sequence of blocks.

packages were installed. The duration of the experiments was planned for 1, 3, and 5 years and was followed by excavation. The ABM aimed to use different buffer materials (mostly bentonites) packed on top of each other. Nine different commercially mined bentonites and two different marine clays were used in ABM I–III. The denotations, abbreviations, and origins of the bentonites and marine clays are as follows: the bentonites were MX80 (Wyoming, USA), Kunigel V1 (JNB, Tsukinuno, Japan), Calcigel (CAL, Bavaria, Germany), Ibeco Seal M-90 (IBE, Askana, Georgia/CIS), Febex (Almeria, Spain), Ikosorb (IKO, Mount Tidienit, Morocco), Rokle (Czech Republic), Asha 505 (Kutch, India), and Deponit CAN (Dep. CAN, Milos, Greece) and the marine clays were Friedland (Neubrandenburg, Germany) and Callovo-Oxfordian (COX, Meuse/Haute-Marne, France). Eleven different clays were compacted into rings (with the exception of four steel cages that contained granulated MX80 and two trimmed discs of solid clay stone material) positioned on top of each other and encapsulating the tube. All the reference (REF) materials, except the MX80 bentonite and the Callovo-Oxfordian clay (COX), were installed two times in the test package and all but the MX80 and COX discs were separated by other blocks (Figure 1). The MX80 bentonite was installed six times as a pure compacted MX80 block, two times as a cage filled with MX80 granulate, and two times as a cage filled with 'MX80 granulate + quartz.' The COX marine clay was installed twice as a compacted block (16, 19) and once as a unit of two trimmed discs of approximately 3–5 cm height each packed on top of each other (20a, 20b). The $EC_{populations}$ in the different REF materials were significantly different. The second out of the three 'ABM packages' (ABM-II) was first allowed to saturate with water for about 2.5 years and then heated for about 3–4 years. This differs from ABM-I which was heated from the start and reached the maximum temperature after about one year (recorded with a temperature sensor 5 mm from the tube). The total duration of the heating was about one year in ABM-I with an intermediate cooling time. The cooling time had a technical purpose and the aim was to avoid boiling. After emplacement of the ABM packages, a slot of ~10 mm thickness between the package and the rock was filled with sand to allow inflowing groundwater to be distributed uniformly around the bentonite

https://doi.org/10.1346/CCMN.2017.064052 Published online by Cambridge University Press

rings. Groundwater was added using two sources: (1) natural inflow from the rock into each of the test holes with an approximately 0.06 L/min flow rate (Eng *et al.*, 2007) and through (2) an artificial water saturation system that was installed in ABM I–III. The titanium pipes used to supply the bentonite blocks with water from a tank in the gallery above the packages contained 120 holes in ABM-I and only 12 holes in ABM-II and ABM-III. Accordingly, more water was allowed to enter ABM-I within the early phase. The nearly neutral pH Äspö water used for artificial saturation was a Na-Ca-Cl dominated groundwater (~2500 mg/L Na^+ and Ca^{2+}, ~8500 mg/L Cl^-, and ~500 mg/L SO_4^{2-}) with minor contents of Mg^{2+}, Br^-, and K^+ (all <100 mg/L). Upon dismantling of the ABM-II package, some of the blocks were found to be more fragile than in the ABM-I package and thus could not be sampled intact (Kumpulainen *et al.*, 2016). The SKB (2014) described the rock surrounding ABM-II as highly fractured. Kaufhold *et al.* (2017a) described samples taken from the ABM-II package with features that indicate disintegration and had traces of halite. They concluded that boiling possibly occurred in the warmest part of the experiment. In both experiments, the buffer materials were exposed to a maximum temperature of 130–141ºC. The temperature distribution, however, was not homogenous and the peak temperatures were recorded by sensors in the buffer at a few cm distance from the heater. The ABM-II was terminated and analyzed for mineralogical/geochemical changes and particularly for ion exchange reactions. Most of the geochemical and mineralogical alterations of the different bentonites (apart from the ECs, anhydrite, and halite precipitation) were restricted to the contacts between iron heater and the bentonite (Kaufhold *et al.*, 2017a). Cation exchange processes, however, were not examined in that study. Kumpulainen *et al.* (2016) studied four out of the thirty-one compacted blocks made of MX80, Deponit CaN (Dep. CAN), and Friedland clay (FRI) in the lower part of the ABM-II package (blocks 2, 4-6). The authors identified an increase in the exchangeable Ca^{2+} and a decrease in the exchangeable Na^+, Mg^{2+}, and K^+, whereas the CECs did not change. No horizontal variations could be identified for the ECs and the CECs. This study was limited to a few blocks in the bottom of ABM-II and was not designed to give information about overall changes in the $EC_{populations}$ of the whole package. In the present study, all blocks were sampled and investigated which was required to understand the processes that occurred in ABM-II.

Sampling

After excavation, the blocks were sampled at different distances from the contact to the iron tube (Figure 1) to allow horizontal variations in the buffer materials between the heater and the rock to be studied. A 2-g sample of material was required to perform the analytical work needed for this study. The samples labelled '0.1 cm' were collected by scraping off the several cm^2 of the surface layer of bentonite blocks at the contact with the iron tube using a sharp knife. Some blocks were in good shape and some blocks were partly disintegrated. In order to collect 2 g of material at a horizontal distance of 2 cm from the heater, 3 holes each at a 2 cm distance were drilled and the materials were mixed together in order to get an overview of the whole block thickness. If blocks were partly disintegrated, the sample mass was collected using more than 3 holes at the same distance. This procedure was repeated for each of the 5 cm and 8 cm samples (compare to Figure 1c). The block pieces could not be sampled uniformly because some were fragmented. Therefore, any possible vertical gradients that might have occurred within single blocks could not be investigated based on this sample set. According to Kaufhold *et al.* (2013) and Dohrmann *et al.* (2013b), vertical gradients within single blocks were expected to be small. Excavation of the ABM experiment could not be performed in an O_2-free atmosphere and, therefore, no glove box was used in the laboratory. In addition to the reacted samples, the REF materials were also analyzed or data were taken from former studies (*e.g.* Kaufhold *et al.*, 2013, Dohrmann *et al.*, 2013b).

CEC and EC methods

The CEC was determined using the Cu-trien$_{5\times calcite}$ method (Dohrmann and Kaufhold, 2009), which uses the Cu-trien index cation that was introduced in the CEC method by Meier and Kahr (1999). In interlaboratory round robin tests, the Cu-trien index cation provided accurate CEC and $EC_{population}$ values even for calcareous bentonites (Dohrmann *et al.*, 2012a, 2012b) and particularly for the exchangeable Ca^{2+} values if the Cu-trien$_{5\times calcite}$ variant of the method was used. The Cu-trien$_{5\times calcite}$ solution suppresses calcite dissolution during the exchange reaction (Dohrmann and Kaufhold, 2009). The Cu-trien$_{5\times calcite}$ solution was prepared by mixing 2000 mL of 0.01 M Cu–trien solution with a controlled Cu:trien ratio (compare to Stanjek and Künkel, 2016) and with 2 g of fine-grained calcite added to saturate the solution with dissolved calcite as described by Dohrmann (2006) and Dohrmann and Kaufhold (2009). Two different sample masses were used (200 mg and 300 mg) and 30.0 mL of Cu-trien$_{5\times calcite}$ exchange solution was added to each sample in an 85 mL centrifuge tube. The slurry was allowed to equilibrate for 2 h in an end-over-end shaker. After Cu-trien$_{5\times calcite}$ saturation, the solutions were centrifuged to sediment the bentonites and the supernatant solutions were diluted and analysed using inductively coupled plasma (ICP) spectrometry with a Thermo Scientific ICAP 6300 DUO ICP-OES (Thermo Fisher Scientific, Waltham, Massachusetts, USA) to measure the ECs, Cu, and allow the calculation of CEC

https://doi.org/10.1346/CCMN.2017.064052 Published online by Cambridge University Press

values. For ICP-OEC analysis, the following techniques were used: argon radial plasma, nebulisers (cross-flow and modified Lichte), no auxiliary gas flow, gain value for plasma (1.400 W), calibration every 7th measurement. The Cu-trien complex concentration was also analyzed using VIS spectroscopy (Jenway 6200, Cole-Parmer, Staffordshire, UK) to cross-check the ICP-Cu concentration. Each CEC value was calculated by averaging four single CEC values (two from ICP analysis and two from VIS spectroscopy). Each EC value was calculated by averaging only two single EC values measured using ICP. The error (± 3 sigma) of the values determined using the Cu-trien$_{5\times calcite}$ method for bentonites (Dohrmann and Kaufhold, 2009) was different for each of the exchangeable cations and the CEC. The scattering of exchangeable cation values was lowest for K^+ (±0.3 meq/100 g), followed by Mg^{2+} (±0.8 meq/100 g), Ca^{2+} (±0.8 meq/100 g), Na^+ (±1.9 meq/100 g), and the CEC (±3.1 meq/100 g). No sample had significant exchangeable Fe (all <0.1 meq/100 g Fe^{3+}) and ECs were measured in meq/100 g. The ECs of the different materials were calculated as a percent of the measured CEC value to make the EC values comparable. In cases where the sum of exchangeable cations was >100%, the presence of typical soluble phases, such as gypsum, was indicated. The Cu-trien$_{5\times calcite}$ approach does not prevent dissolution of gypsum (Dohrmann and Kaufhold, 2010). The parameter "sum-CEC" indicates soluble minerals, such as Ca-sulfates or halite, if the value is positive, but it may also indicate salts from evaporated pore water (compare to Dohrmann et al., 2012b). For pH measurements, dispersions were produced using 1 g of solid and 50 mL deionized water (2% dispersion) and measured after 5 min stirring using a standard pH electrode. In this study, the expression 'horizontal variation' was used for EC and CEC values at distances between 2 and 8 cm from the heater because this part was representative of the bulk of the blocks. The 0.1 cm sample on the other hand was important in understanding processes at the bentonite/heater interface, however, the contribution of this thin layer to the bulk composition was low. All of the following EC and CEC values refer to samples from different parts of individual blocks or the average values from different blocks (Table 1).

RESULTS AND DISCUSSION

Horizontal variation of the CECs and the ECs within individual blocks

As expected from ABM-I (Kumpulainen and Kiviranta, 2011; Svensson *et al*., 2013; Dohrmann *et al*., 2013b), all blocks in the ABM-II experiment showed large variations in the CEC and EC values (except for exchangeable K^+) of the REF (pristine material) and the reacted samples (Table S1 in the Supplemental Materials section (deposited with the Editor-in-Chief and available at http://www.clays.org/JOURNAL/JournalDeposits.html)). The horizontal variations in the CEC and the $EC_{population}$ values within individual blocks ($CEC_{(individual\ 2-8\ cm)}$, $EC_{population,\ (individual\ 2-8\ cm)}$) was expected to be similarly low as in ABM-I (Dohrmann *et al*., 2013b) because the maximum temperatures in both the ABM-I and ABM-II experiments were similar, but the time duration of the heating in ABM-II was even longer than ABM-I and allowed more time to approach equilibrium conditions. Six blocks from different depths in the ABM-II package were selected to examine the typical horizontal variations. Rokle was selected twice because one of the Rokle blocks was located in a zone that may have been affected by boiling as reported and discussed by Kaufhold *et al*. (2017a). For some blocks, either no variations existed or no systematic horizontal variations in the $CEC_{(individual\ 2-8\ cm)}$ and the $EC_{population\ (individual\ 2-8\ cm)}$ values were observed (*e.g.* block 1 in Figure 2). Most blocks lost exchangeable

Table 1. The blocks and sampling distances from heaters in ABM-II used to calculate the EC (Na^+, Mg^{2+}, or Ca^{2+}) and CEC values.

Horizontal profile, individual block, 0.1 cm	$EC_{(ind.\ 0.1\ cm)}$	$CEC_{(ind.\ 0.1\ cm)}$
Horizontal profile, individual block, from 2−8 cm	$EC_{(ind.\ 2-8\ cm)}$	$CEC_{(ind.\ 2-8\ cm)}$
Average value of individual block, from 2−8 cm	$EC_{(av.\ 2-8\ cm)}$	$CEC_{(av.\ 2-8\ cm)}$
Average value of blocks 1−31, at 0.1 cm	$EC_{(av.\ blocks\ 1-31,\ 0.1\ cm)}$	$CEC_{(av.\ blocks\ 1-31,\ 0.1\ cm)}$
Average value of blocks 1−31, at 2 cm	$EC_{(av.\ blocks\ 1-31,\ 2\ cm)}$	$CEC_{(av.\ blocks\ 1-31,\ 2\ cm)}$
Average value of blocks 1−31, at 5 cm	$EC_{(av.\ blocks\ 1-31,\ 5\ cm)}$	$CEC_{(av.\ blocks\ 1-31,\ 5\ cm)}$
Average value of blocks 1−31, at 8 cm	$EC_{(av.\ blocks\ 1-31,\ 8\ cm)}$	$CEC_{(av.\ blocks\ 1-31,\ 8\ cm)}$
Average value of blocks 1−31, from 2−8 cm	$EC_{av.\ blocks\ 1-31,\ 2-8\ cm}$	$CEC_{av.\ blocks\ 1-31,\ 2-8\ cm}$
Average value of blocks 1−10, from 2−8 cm	$EC_{(av.\ lower)}$	$CEC_{(av.\ lower)}$
Average value of blocks 11−21, from 2−8 cm	$EC_{(av.\ middle)}$	$CEC_{(av.\ middle)}$
Average value of blocks 22−31, from 2−8 cm	$EC_{(av.\ upper)}$	$CEC_{(av.\ upper)}$

https://doi.org/10.1346/CCMN.2017.064052 Published online by Cambridge University Press

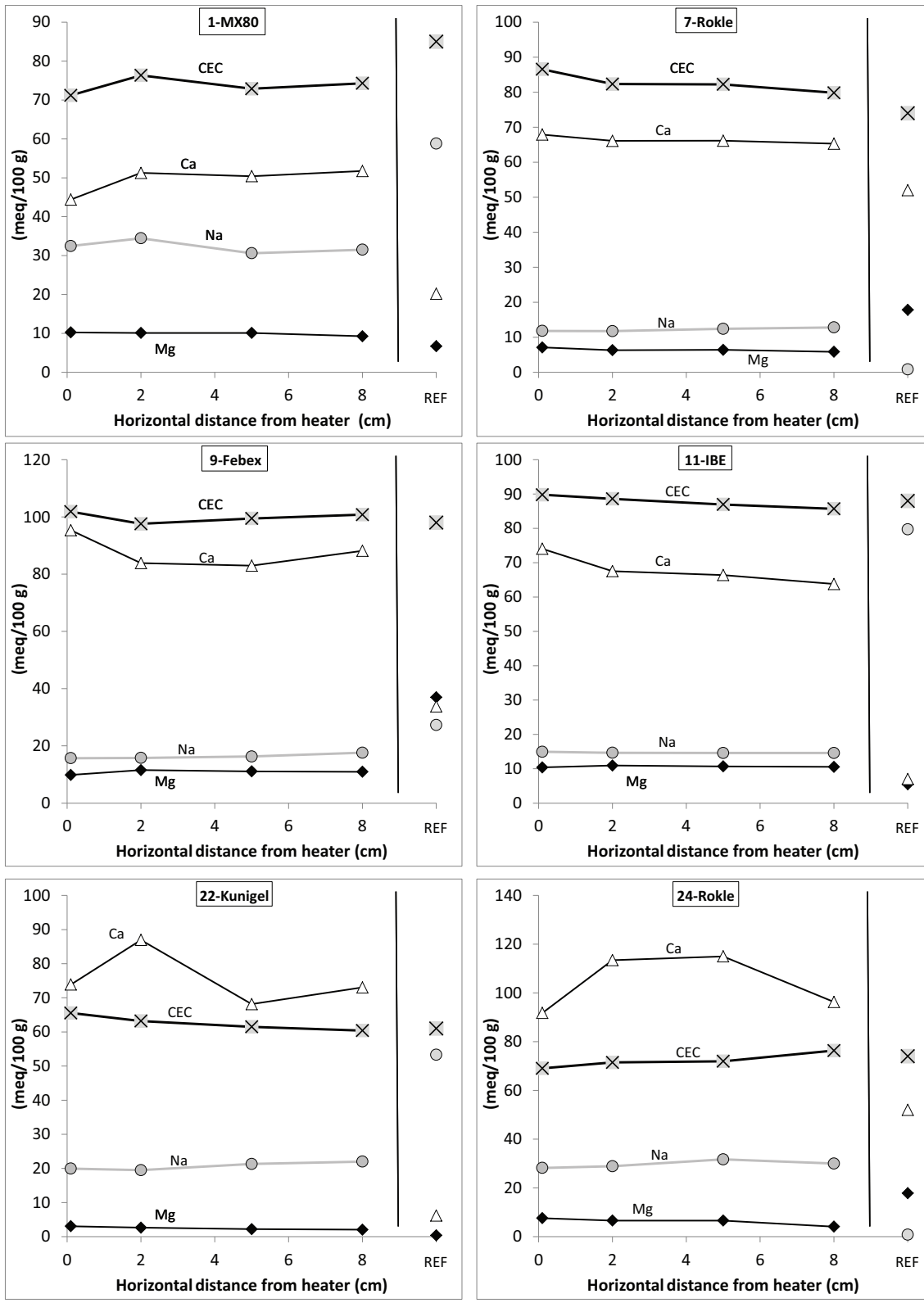

Figure 2. Examples of the different $EC_{(individual\ 2-8\ cm)}$ and $CEC_{(individual\ 2-8\ cm)}$ distributions of the different blocks. The block numbers are indicated in the label boxes at the top of each graph before the sample name: 1- MX80, 7- Rokle; 9- Febex; 11- IBE; 22- Kunigel; 24- Rokle.

https://doi.org/10.1346/CCMN.2017.064052 Published online by Cambridge University Press

$Na^{+}_{(individual\ 2-8\ cm)}$. Exchangeable $Na^{+}_{(individual\ 2-8\ cm)}$ showed no horizontal variations in the lower part of ABM-II (with the exception of blocks 1 and 2, which were close to the cement plug). In the upper part, exchangeable $Na^{+}_{(individual\ 2-8\ cm)}$ showed minor horizontal changes in single blocks. The $Na^{+}_{(individual\ 2-8\ cm)}$ values decreased towards the heater side (from 8 cm to 2 cm) of blocks 21–22 and 24–28. Only in the 2 cm sample of block 23 in the middle of this sequence were much larger $Na^{+}_{(individual\ 2-8\ cm)}$ values detected. This sample contained halite (Kaufhold *et al*., 2017a), which was dissolved during the CEC experiment and inflated the $Na^{+}_{(individual\ 2-8\ cm)}$ values (*i.e*. exchangeable Na^{+} plus Na^{+} from dissolved halite). The total differences between the exchangeable $Na^{+}_{(individual\ 2-8\ cm)}$ values in the horizontal direction were relatively low. In block 21 for example, the $Na^{+}_{(individual\ 2-8\ cm)}$ values decreased from 25 (at 8 cm) to 22 (at 2 cm) meq/100 g (Table S1 in Supplemental Materials section). No horizontal changes in the exchangeable $Mg^{2+}_{(individual\ 2-8\ cm)}$ values were detected in the middle part (Table 2b) of ABM-II and in the two top blocks (blocks 30–31) close to the cement plug. In some blocks, however, exchangeable $Mg^{2+}_{(individual\ 2-8\ cm)}$ values increased by 1–2 meq/100 g towards the heater side, particularly in the upper part (blocks 15–29, Tables 2 and 3; compare to Figure 2, blocks 22 and 24) and in the lower part (blocks 1–6, Table S1 in Supplemental Materials section). This trend

Table 2. Average values (a) in vertical gradients (0.1–8 cm) over the whole ABM-II package with the EC, sum of EC, and CEC Cu-trien$_{5xcalcite}$ values (meq/100 g) of all the ABM-II samples including the reference (REF) samples taken from Table 1. The whole package (b) which included blocks 1–31 was further subdivided into three parts (lower, middle, and upper). The total gains and losses in EC and CEC were calculated in % with respect to the reference values. Note that blocks 19 and 20 were disintegrated and could not be analyzed.

Distance (cm)	Na^{+}	K^{+}	Mg^{2+}	Ca^{2+}	sum	CEC
	(meq/100 g)					
a						
Blocks 1–31 (whole ABM-II package)						
REF	41	2	12	24	76	74
0.1	17	1	6	75	99	73
2	18	1	5	72	97	74
5	18	1	5	68	92	73
8	18	1	5	67	90	72
Average loss (–)/gain (+) (%/REF)						
2–8	–56	–	–59	+192	+22	–2
b	3 segments (lower, middle, upper part)					
Blocks 22–31 – upper						
REF	39	2	14	25	76	74
0.1	19	2	4	80	104	72
2	20	1	3	85	109	72
5	20	1	3	79	103	72
8	21	1	2	76	100	72
Blocks 11–21 – middle						
REF	48	2	9	16	73	71
0.1	15	1	5	81	102	74
2	16	1	5	69	90	72
5	16	1	5	64	86	71
8	16	1	5	64	86	70
Blocks 1–10 – lower						
REF	36	2	14	30	79	78
0.1	17	1	8	65	90	75
2	18	1	8	63	90	76
5	18	1	8	61	87	76
8	18	1	7	60	86	75

https://doi.org/10.1346/CCMN.2017.064052 Published online by Cambridge University Press

Table 3. The 2−8 cm sample average EC (%), CEC, and "sum-CEC" values (meq/100 g) of the ABM-II samples measured using the Cu-trien$_{5xcalcite}$ method. Note that the "exchangeable Ca^{2+}" values often were inflated by soluble sulfate minerals.

			REF material					Reacted samples 2−8 cm (averages)					
Block		Material/abbreviation	Na^+	K^+	Mg^{2+}	Ca^{2+}	CEC	Na^+	K^+	Mg^{2+}	Ca^{2+}	CEC	sum-CEC
			(%)				(meq/100 g)	(%)				(meq/100 g)	
31		MX80	69	2	8	24	85	41	2	4	70	78	13
30		MX80	69	2	8	24	85	23	1	3	89	77	14
29		Febex	27	3	37	33	101	16	2	4	92	98	13
28		Ikosorb (IKO)	56	2	24	19	90	15	1	3	107	88	24
27	cage	MX80 granulate	69	2	8	24	85	20	< 1	2	109	81	26
26		Dep. CAN	27	2	27	46	84	19	1	2	126	83	42
25	cage	MX80 granulate+quartz	69	2	8	24	59	26	<1	4	108	56	21
24		Rokle (Rawra)	1	3	24	71	74	41	2	8	148	73	71
23		Friedland (FRI)	69	8	22	2	23	83	7	9	222	24	59
22		Kunigel V1 (JNB)	94	1	2	7	61	34	1	4	123	62	38
21		Asha 505	67	1	15	20	91	28	1	5	125	83	45
20	a,b	Callovo-Oxfordian discs	24	11	29	35	12	Disintegrated blocks					
19		Callovo-Oxfordian											
18		Calcigel (CAL)	3	2	22	72	65	31	2	6	98	68	25
17		MX80	69	2	8	24	85	25	1	5	98	81	24
16		Callovo-Oxfordian	24	11	29	35	12	35	9	12	129	13	12
15		Ibeco Seal (IBE)	90	4	6	8	88	23	2	6	84	87	12
14	cage	MX80 granulate+quartz	69	2	8	24	59	21	<1	8	89	61	11
13		Kunigel V1 (JNB)	94	1	2	7	61	19	1	7	80	65	4
12		Ikosorb (IKO)	56	2	24	19	90	16	<1	7	83	95	5
11		Ibeco Seal (IBE)	90	4	6	8	88	17	2	12	76	87	6
10		Asha 505	67	1	15	20	91	16	1	13	82	89	10
9		Febex	27	3	37	33	101	17	2	8	86	99	12
8	cage	MX80 granulate	69	2	8	24	85	16	<1	6	89	85	10
7		Rokle (Rawra)	1	3	24	71	74	15	<1	8	81	82	3
6		MX80	69	2	8	24	85	16	<1	8	88	83	10
5		Dep. CAN	27	2	27	46	84	19	<1	8	86	83	11
4		Friedland (FRI)	69	8	22	2	23	37	6	10	121	23	17
3		Calcigel (CAL)	3	2	22	72	65	36	2	16	64	64	11
2		MX80	69	2	8	24	85	42	<1	13	67	75	16
1		MX80	69	2	8	24	85	43	<1	13	69	75	19

was weak because the differences were close to the detection limit. In ten blocks, no significant horizontal changes were observed for exchangeable $Ca^{2+}_{(individual\ 2-8\ cm)}$ values: blocks 1−3, 7, 10, 15−16, 18, 25, and 29. In three blocks the trend was not clear (blocks 21, 22, and 24). In two blocks (9 and 23) exchangeable $Ca^{2+}_{(individual\ 2-8\ cm)}$ values were larger closer to the rock side. In the remaining fourteen out of thirty-one blocks, however, exchangeable $Ca^{2+}_{(individual\ 2-8\ cm)}$ values increased towards the heater side in the horizontal direction from 8−2 cm: blocks 4−6, 8, 11−14, 17, 26−28, and 30−31. The highest absolute exchangeable $Ca^{2+}_{(individual\ 2-8\ cm)}$ values were detected in the upper part of ABM-II. In the upper part of ABM-II, exchangeable $Ca^{2+}_{(individual\ 2-8\ cm)}$ values (76−85 meq/100 g) exceeded the CEC values (72 meq/100 g) which differed from ABM-I (Table 2). The exchangeable $K^{+}_{(individual\ 2-8\ cm)}$ values were usually too small and close to the detection limit to clearly identify any changes. A steady horizontal increase in the $CEC_{(individual\ 2-8\ cm)}$ values from 2−8 cm with decreased distance from the heater was observed in blocks 7 and 11 (Figure 2) and blocks 2, 3, 5, 6, 7, 11, 12, 17, 18, 22, 26, and 30−31. Rarely, the opposite trend was observed with a slight decrease in $CEC_{(individual\ 2-8\ cm)}$ values with decreased distance from the heater (block 24, Figure 2). In the other blocks, variations in the $CEC_{(individual\ 2-8\ cm)}$ values were either negligible or did not show a clear horizontal trend. Summing up, the first hypothesis had to be rejected because horizontal differences in EC and CEC values were detected in ABM-II. The question arose as to how these differences in ECs and CECs developed.

Horizontal variation of the CECs and the ECs on a larger scale

In ABM-I, no horizontal changes were detected and single values for all ECs and the CEC were calculated to represent a single block ($CEC/EC_{(av.\ 2-8\ cm)}$). In ABM-II, horizontal changes in single blocks were observed ($CEC/EC_{(individual\ 2-8\ cm)}$), however, an examination of the horizontal changes in these single blocks failed to help understand the trends. To obtain an overview of large scale exchange processes in ABM-II, the average

https://doi.org/10.1346/CCMN.2017.064052 Published online by Cambridge University Press

values of horizontal changes in CEC and EC were calculated: (1) for all blocks from 2–8 cm ($CEC/EC_{(av.\ blocks\ 1-31,\ 2-8\ cm)}$); (2) for all blocks at each distance from the heater ($CEC/EC_{(av.\ blocks\ 1-31,\ 0.1\ cm,\ 2\ cm,\ 5\ cm,\ 8\ cm)}$) (Table 2a); and averages of the ECs and CECs at horizontal distances of 0.1, 2, 5, and 8 cm were also calculated for (3) units that consisted of approximately ten blocks (upper (22–31), middle (11–21), and lower part (1–10), $CEC/EC_{(av.\ upper,\ middle,\ lower)}$, Table 2b). One must note that the average EC and CEC values also depended on the type of materials. The $EC_{population}$ in most of the blocks, however, was modified during the experiment. In total, the exchangeable $Na^{+}_{(av.\ blocks\ 1-31,\ 2-8\ cm)}$ and $Mg^{2+}_{(av.\ blocks\ 1-31,\ 2-8\ cm)}$ values decreased in ABM-II by approximately 55% (59%), whereas the exchangeable $Ca^{2+}_{(av.\ blocks\ 1-31,\ 2-8\ cm)}$ values increased by approximately 200%. Horizontal changes in all blocks at each distance could only be detected for exchangeable $Ca^{2+}_{(av.\ blocks\ 1-31,\ 0{,}1\ cm,\ 2\ cm,\ 5\ cm,\ 8\ cm)}$) with a trend of increased exchangeable Ca^{2+} concentrations as the distance from the rock to the heater decreased. The largest losses were observed for exchangeable Na^{+} in the middle part (−67% exchangeable $Na^{+}_{(av.\ middle)}$), in comparison to the upper and lower parts (−51% and −50% exchangeable $Na^{+}_{(av.\ upper,\ lower)}$). The average losses of $Mg^{2+}_{(av.\ middle)}$ and $Mg^{2+}_{(av.\ lower)}$ were similar for the middle and the lower parts of ABM-II (43% and 44%, respectively). In the upper part, the exchangeable $Mg^{2+}_{(av.\ upper)}$ values decreased by 79%. The warmer parts that were closer to the heater (2 cm) had larger $Ca^{2+}_{(av.\ blocks\ 1-31,\ 2\ cm)}$ values and the smallest differences in $Ca^{2+}_{(av.\ lower)}$ in the horizontal direction were found in the lower parts of ABM-II (Table 2b).

Average EC and CEC values in the entire ABM-II package

In order to understand ion exchange processes by interactions with groundwater, the average EC and CEC values ($CEC/EC_{(av.\ 2-8\ cm)}$) in the horizontal samples in all the individual blocks of the reacted ABM-II package were calculated. On this scale, it is more useful to compare the EC values as % values which were calculated as follows: Na (%/CEC) = Na (meq/100 g)/CEC (meq/100 g) and used in Table 3 and Figure 5. Note that this calculation was done for REF materials as well as for reacted samples. The $CEC_{(REF)}$ values were only used for $EC_{(REF)}$ calculation. For EC calculation of reacted samples, the CEC values of the reacted samples were used. Using this calculation, the sum of ECs may exceed the CEC both in the REF materials and the reacted samples. An overview of the differences in the REF materials ($CEC_{(REF)}$, $EC_{(REF)}$) (Table 3) and a comparison of ABM-II to ABM-I were, thus, possible. Exchangeable $Na^{+}_{(av.\ 2-8\ cm)}$ and $Mg^{2+}_{(av.\ 2-8\ cm)}$ values decreased in most blocks in comparison to the starting materials, whereas "exchangeable $Ca^{2+}_{(av.\ 2-8\ cm)}$" values strongly increased (Table 4). For the average $EC_{population}$ in all the analyzed blocks, the $Ca^{2+}_{(av.\ 2-8\ cm)}$ values were highest (100% and certainly inflated partly by dissolution of gypsum or anhydrite), followed by $Na^{+}_{(av.\ 2-8\ cm)}$ (27%), $Mg^{2+}_{(av.\ 2-8\ cm)}$ (7%), and $K^{+}_{(av.\ 2-8\ cm)}$ (2%). Only two bentonites showed an increase in exchangeable $Na^{+}_{(av.\ 2-8\ cm)}$ with respect to the average values and these bentonites had very low $Na^{+}_{(REF)}$ values (Rokle and Calcigel, both <5%). One of the FRI blocks (block 23) and the only intact COX block (block 16) also showed an increase in average $Na^{+}_{(av.\ 2-8\ cm)}$ values (14 % and 11 %, respectively). All other blocks lost exchangeable

Table 4. The observed differences between the ABM-I and ABM-II samples.

Parameter	ABM-I	ABM-II
Heating	From start	After water saturation
Duration of heating phase	1 year	3-4 years
Artificial water sturation by Ti tubes	4 holes per block (120 in total)	4 holes each 10 blocks
No. of blocks	30	31
Horizontal variation (Na^{+})	–	upper part
Horizontal variation (Mg^{2+})	–	upper part
Horizontal variation (Ca^{2+})	–	– (inflated)
Horizontal variation (CEC)	–	–
Na^{+} loss (total)	19%	55%
Mg^{2+} loss (total)	17%	59%
Ca^{2+} gain (total)	41%	~200%
Na^{+} loss (section)	upper part	middle part
Mg^{2+} loss (section)	–	upper part
Ca^{2+} gain (section)	upper part	upper part
CEC drop	stronger than ABM-II, different bentonites	MX80 (4 ×), Asha
Sum-CEC	<5 meq/100 g	~20 meq/100 g, partly inflated
Boiling	–	assumed
Na^{+}/Mg^{2+}-ratio	3.1 (blocks 16–30); 2.9 (blocks 1–15)	5–10 (blocks 16–31); 3.5 (blocks 1–15)

https://doi.org/10.1346/CCMN.2017.064052 Published online by Cambridge University Press

$Na^{+}_{(av.\ 2-8\ cm)}$ and the losses were larger when the concentration of the REF material was high. Also for exchangeable $Mg^{2+}_{(av.\ 2-8\ cm)}$ values, the losses were larger when the concentration of the REF materials was high. Only one out of the measured 29 blocks lost exchangeable $Ca^{2+}_{(av.\ 2-8\ cm)}$ (Calcigel, block 3) and all others were enriched in exchangeable $Ca^{2+}_{(av.\ 2-8\ cm)}$. No correlation was found between the exchangeable $Ca^{2+}_{(REF)}$ values and the gains in exchangeable $Ca^{2+}_{(av.\ 2-8\ cm)}$. As discussed, the exchangeable Ca^{2+} values were difficult to interpret mostly because of (1) variable amounts of at least partially soluble components (such as gypsum or anhydrite) present in many reacted blocks (compare to Kaufhold *et al*., 2017a) which inflated exchangeable Ca^{2+} values; (2) additional exchangeable Ca^{2+} sources may have increased the ionic strength by evaporation of groundwater; and (3) an unknown amount of actual exchangeable Ca^{2+} which was increased by ion exchange. The gypsum and anhydrite concentrations were quantified using the differences between the elemental sulfur concentrations of the reacted samples and the REF samples. Assuming that these minerals were dissolved completely during a CEC experiment, the inflated Ca^{2+} values can be calculated and used to correct the actual exchangeable Ca^{2+} values as discussed by Dohrmann and Kaufhold (2010). In the ABM-II package, however, the increase in measured exchangeable Ca^{2+} values did not correlate with the "calculated inflated exchangeable Ca^{2+}" values based on anhydrite and gypsum dissolution (Figure 4). The problem was discussed for block 21, which was close to the "boiling zone" and the 2 cm sample contained anhydrite (compare to Kaufhold *et al*., 2017a). For this sample, approximately half of the observed increase in exchangeable Ca^{2+} can be explained by anhydrite dissolution, whereas this amount was much lower for the '0.1 cm' sample and anhydrite was absent in the 5 cm and 8 cm samples. In all of these samples of block 21, the sum of exchangeable cations exceeded the measured CEC values by 50% or more. Obviously, soluble Ca-sulfate minerals cannot explain these differences. An alternative source for the "inflated exchangeable Ca^{2+}" values could be the evaporation of groundwater which led to an increased ionic strength. On the other hand, a real increase in actual exchangeable Ca^{2+} was likely as well. The increased measured values of exchangeable Ca^{2+} were correlated with the "exchangeable Ca^{2+}" values that were calculated from anhydrite and gypsum dissolution. Differences in the CEC values between the REF materials and the bulk average values ($CEC_{(av.\ 2-8\ cm)}$) were typically lower than the reproducibility (±3.1 meq/100 g, ±3 sigma) of the applied method. Only a few samples showed larger deviations, such as the two bottom blocks and the two top blocks of MX80 and Asha 505 (block 21) in the boiling zone. The only block that showed a pronounced $CEC_{(av.\ 2-8\ cm)}$ increase was Rokle (block 7, Figure 3). The CEC blocks that showed a decrease could have resulted from (1) structural degradation of the smectites, (2) "dilution" of the sample by the precipitation of secondary minerals, such as anhydrite, which has a very low CEC value, or (3) by pH changes which caused lower CECs by the lower amounts of pH-dependent charge.

The structural degradation of smectites (1) is an unlikely source of the observed CEC decrease. Even for the '0.1 cm' sample, Kaufhold *et al*. (2017a) observed no indication of smectite interstratification for any block in comparison to the REF materials after intercalation with ethylene glycol. No direct ethylene glycol expansion measurements were performed on the samples from 2–8 cm, but the alteration conditions (temperature, corrosion) were less aggressive in this part of the experiment. The CEC of a bentonite may have decreased by "dilution" of the reacted sample in comparison to a REF sample. If secondary low-CEC minerals, such as anhydrite, gypsum, goethite, carbonates, etc., were formed in a sample in ABM-II, then the CEC would be lower. Kaufhold *et al*. (2017a) studied all the samples of ABM-II with particular focus on the dissolution and precipitation of these mineral phases. They concluded that only anhydrite concentrations increased significantly, particularly in the upper part of the package; however, no quantitative analysis was performed. Total S concentrations can be used to calculate the increase in sulfate minerals (anhydrite + gypsum). The calculation was performed in a way that the S concentration of the REF sample was subtracted from an ABM-II sample by assuming that the difference in S content represents anhydrite or gypsum. This procedure fails, however, to take into account pyrite dissolution because pyrite concentrations were very low. The largest S increase in a bentonite material with respect to the REF samples was observed in blocks 21 (Asha 505), 24 (Rokle), and 26 (Dep. CAN) (all 2 cm samples) with an increase of 0.5–0.6% S, which indicates a total mass of 2–3% anhydrite or gypsum. Hence, the resulting CEC values of these samples should be 2–3% lower. The CEC analyses of these particular "2 cm samples" ($CEC_{(2\ cm)}$) gave no clear correlation with −10% (block 21), −3% (block 24), and +1% (block 26). In the top and bottom blocks where up to 10% lower $CEC_{(av.\ 2-8\ cm)}$ values were recorded, the variations in S concentrations were not large enough to explain a CEC decrease by "dilution." The CEC of a bentonite may also be influenced by pH changes. The pH values, however, were only measured for the REF and "contact samples" (0.1 cm) and no information is available to discuss any changes in the $CEC_{(av.\ 2-8\ cm)}$ values of the blocks. For the $CEC_{(0.1\ cm)}$ samples, however, a pH increase could have been caused by corrosion and cation exchange with a pH increase/decrease correlated with increased/decreased Na^{+} values (Kaufhold *et al.*, 2008). A comparison of the $CEC_{(0.1\ cm)}$ decrease with the pH change indicated that part of the $CEC_{(0.1\ cm)}$ decrease

https://doi.org/10.1346/CCMN.2017.064052 Published online by Cambridge University Press

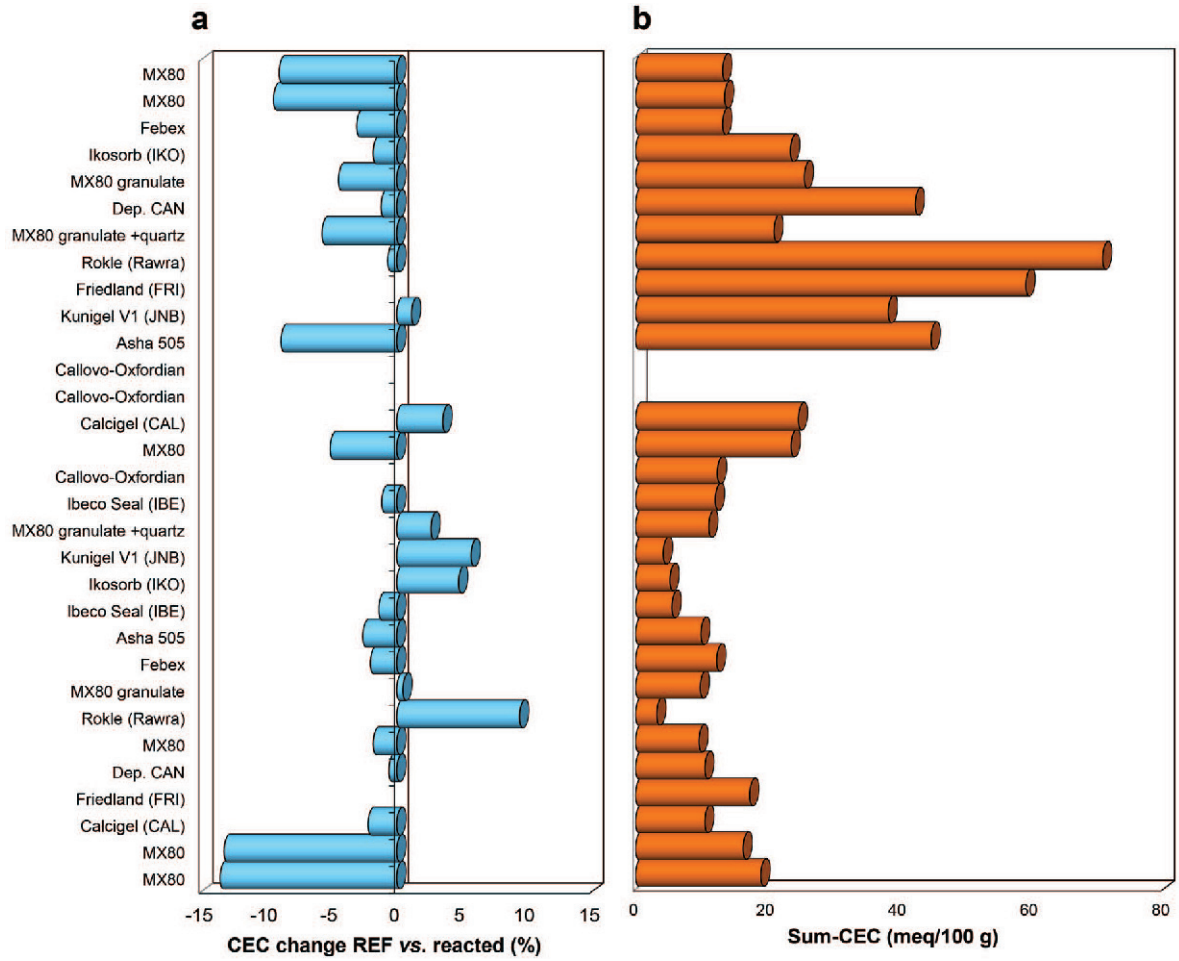

Figure 3. Bar graphs to indicate (a) the CEC changes of the REF samples *vs*. the reacted samples and (b) the sum of the ECs - CEC (sum − CEC) values at the end of the test for the 2−8 cm samples (averages) for all blocks of ABM-II.

can be explained by the decrease in pH. The trend, however, was weak and suggested that, in addition, other reactions were involved that affected the $CEC_{(0.1\ cm)}$. Examples of such additional reactions could be the oxidation of ferrous Fe and the precipitation of Fe (oxyhydr)oxides because the reacted samples had been oxidized. The $CEC_{(0.1\ cm)}$ decrease for the MX80 samples correlated with the pH decrease from 10.0 to 8.5−9.5, but similar decreases in pH were also found in Calcigel, block 18 for samples with an increase in $CEC_{(0.1\ cm)}$. Based on the analyzed data, this $CEC_{(0.1\ cm)}$ decrease cannot yet be explained. The parameter "sum-CEC" indicated soluble minerals, such as sulfates or halite for a positive value (compare to Dohrmann *et al.*, 2012b). Calcite and dolomite dissolution was minimized in this study using the Cu-$trien_{5\times calcite}$ CEC method. As discussed before, gypsum, anhydrite, and in part halite were responsible for the inflated exchangeable Na^+ and Ca^{2+} values and, therefore, the inflated "sum-$CEC_{(av.\ 2-8\ cm)}$" values (Figure 3). In general, the "sum-$CEC_{(av.\ 2-8\ cm)}$" values were <20 meq/100 g in the lower part of the ABM-II package. The "sum-$CEC_{(av.\ 2-8\ cm)}$" increased strongly in the upper part of the ABM-II package close to the disintegrated blocks (19−20) and decreased again to values around 20 meq/100 g in the top blocks (29−31).

This trend can be followed by the changes in the $Ca^{2+}_{(av.\ 2-8\ cm)}$ values of the $EC_{population}$ (Table 3). The values were always >100% in the upper part (blocks 16, and 21−28) and were >100% only once in the lower part of block 4, FRI, which had a low CEC value. Summing up, the second hypothesis that the exchangeable cation ratios were equal in all blocks independent of position has to be rejected because the $Ca^{2+}_{(av.\ 2-8\ cm)}$:$Na^{+}_{(av.\ 2-8\ cm)}$:$Mg^{2+}_{(av.\ 2-8\ cm)}$ ratios were not equal in all blocks of ABM-II, independent of position in the package. Instead, large variations were present and these variations were even more pronounced in the vicinity of the two disintegrated blocks (19 and 20).

Exchangeable cation redistribution over the entire ABM-II package and Na^+/Mg^{2+}-ratios

The question arose as to why equilibrium was not reached or if equilibrium was reached why did the

https://doi.org/10.1346/CCMN.2017.064052 Published online by Cambridge University Press

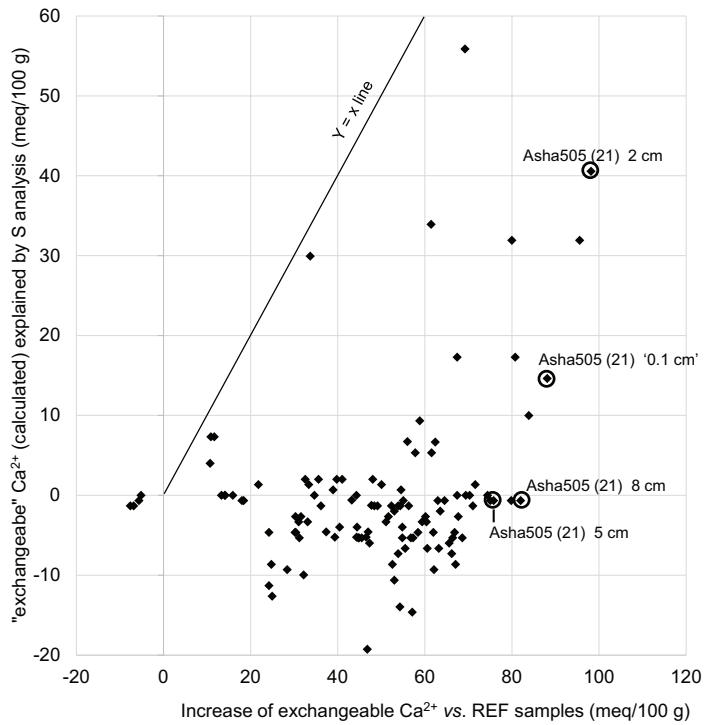

Figure 4. Correlation between the measured increases in exchangeable Ca^{2+} values and the calculated "exchangeable Ca^{2+}" values from anhydrite and gypsum dissolution.

equilibrium change. Exchangeable Na^+ and Mg^{2+} values were not inflated by soluble minerals with the one exception of halite in block 23. Therefore, the Na^+/Mg^{2+}-ratio and the gains and losses in $Na^+_{(av.\ 2-8\ cm)}$ and $Mg^{2+}_{(av.\ 2-8\ cm)}$ values (Na^+/Mg^{2+}-$ratio_{(av.\ 2-8\ cm)}$) were investigated in more detail (Figure 5). After installation and before the heating of ABM-II, the Na^+/Mg^{2+}-$ratios_{(REF)}$ of the REF samples varied from <0.1 (Rokle) to 47 (Kunigel V1). Fourteen bentonites had Na^+/Mg^{2+} $ratios_{(av.\ 2-8\ cm)}$ >5 (two blocks of Kunigel V1, two blocks of IBE, and ten blocks of MX80). These blocks were evenly distributed from bottom to the top of ABM-II. During the experiment, the blocks took up groundwater while being heated. After retrieval, however, a clear distinction could be made between the Na^+/Mg^{2+} $ratios_{(av.\ 2-8\ cm)}$ of the upper and lower part of the package. In the upper part (block numbers >15), a significant variation in the Na^+/Mg^{2+} $ratios_{(av.\ 2-8\ cm)}$ and the larger absolute Na^+/Mg^{2+} $ratios_{(av.\ 2-8\ cm)}$ were observed and ranged from approximately 5 to 10 (Figure 5). In the lower part (blocks 1–15), the Na^+/Mg^{2+} $ratio_{(av.\ 2-8\ cm)}$ was on average 3.5 with little variation. This indicated that locally different conditions affected the cation equilibration.

Comparison of ABM-II with ABM-I

In ABM-II, heating of the package started after water saturation, whereas heating in ABM-I started immediately after installation. The duration of heating was longer in ABM-II (3–4 years) than in ABM-I (approximately 1 year). Before ABM-II and during the heating of both ABM-I and ABM-II, groundwater interacted with the blocks. The question was whether or not this groundwater interaction influenced equilibrium of the $EC_{population}$ in the two packages. Note that ABM-II and ABM-I had the same buffer materials, but were packed in different sequences. This created many different interfaces and EC gradients. Even in ABM-I after 2.5 years of heating, Dohrmann *et al*. (2013b) showed that the $EC_{population}$ was almost completely equilibrated with the surrounding water and this was confirmed by modelling (Wallis *et al*., 2016). As heating was even longer in ABM-II, the equilibration should not be significantly influenced by the block sequences. The observed differences between ABM-I and ABM-II were summarized (Table 4) and are discussed below. In contrast to the previous field study in ABM-I (Dohrmann *et al*., 2013b Sasamoto *et al*., 2017), horizontal variations in the $EC_{population}$ in single blocks of ABM-II could be observed. The Ca^{2+}-rich Äspö water diffused in from the rock side and caused a decrease in the exchangeable Na^+ and Mg^{2+} values and an increase in the Ca^{2+} values in ABM-II. The expected gradient (if observed) should show larger $Ca^{2+}_{(individual\ 2-8\ cm)}$ values closer to the rock. This would mean that $Na^+_{(individual\ 2-8\ cm)}$ values were lower closer to the rock. In some blocks in the upper part, however, the $Na^+_{(individual\ 2-8\ cm)}$ values were lower close to the heater

https://doi.org/10.1346/CCMN.2017.064052 Published online by Cambridge University Press

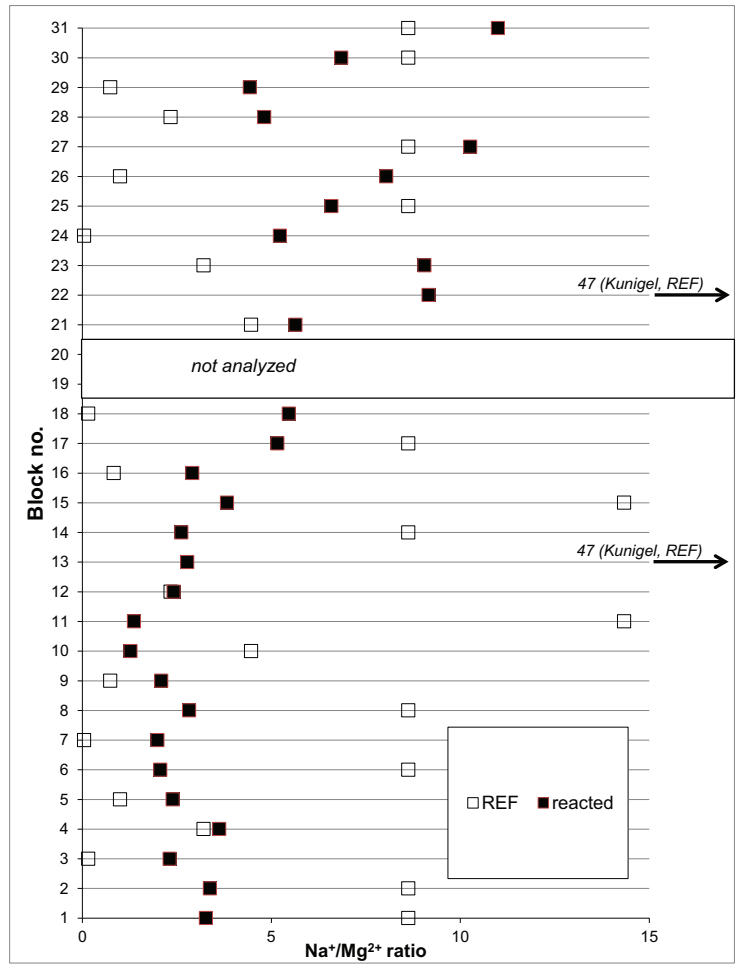

Figure 5. Plot of block number versus Na^+/Mg^{2+} ratios for exchangeable $Na^+_{(av.\ 2-8\ cm)}$ and $Mg^{2+}_{(av.\ 2-8\ cm)}$ (filled squares) in ABM-II of reacted samples in comparison to the Na^+/Mg^{2+} ratios for the REF samples (open squares).

(blocks 21–22 and 24–28, Table 2a). In the rest of the ABM-II package, the $Na^+_{(individual\ 2-8\ cm)}$ values showed no changes or relatively low horizontal changes between 8 and 2 cm from the rock side to the contact with the iron heater. The $Mg^{2+}_{(individual\ 2-8\ cm)}$ values were more or less equal in the horizontal direction in the middle and lower parts of ABM-II, whereas the horizontal changes in the upper part were visible and indicated larger $Mg^{2+}_{(individual\ 2-8\ cm)}$ values towards the heater. The ABM-II blocks were enriched in "exchangeable Ca^{2+}" (partly inflated). The warmer parts had larger $Ca^{2+}_{(av.\ blocks\ 1-31,\ 2\ cm)}$ values and the smallest differences in values with horizontal position were found in the lower part of ABM-II. A steady increase in $CEC_{(individual\ 2\ cm,\ 5\ cm,\ 8\ cm)}$ values towards the heater side was observed in blocks 7 and 11, however, in most blocks the variation in CEC values was either negligible or without a clear horizontal trend. Dividing ABM-II into three units of ten blocks each gives interesting insights into the large scale horizontal changes (gains and losses of $Na^+_{(av.\ upper,\ middle,\ lower)}$, $Mg^{2+}_{(av.\ upper,\ middle,\ lower)}$, and $Ca^{2+}_{(av.\ upper,\ middle,\ lower)}$) that were missing in ABM-I. The total exchangeable Na^+ and Mg^{2+} values decreased by approximately 55% and 59% in ABM-II. The largest total loss of exchangeable Na^+ was observed in the middle part (−67%), whereas the exchangeable Mg^{2+} values decreased by 79% in the upper part. In contrast to these large absolute losses, the Na^+ and Mg^{2+} values showed only minor horizontal variations in the three parts of ABM-II. Total exchangeable Ca^{2+} values increased by nearly 200% in ABM-II and the highest values were measured in the top section. The exchangeable Ca^{2+} increase cannot be evaluated precisely with respect to mass balances because the method used to determine CEC cannot avoid artefacts caused by the dissolution of soluble Ca-sulfates. As already established in ABM-I, average values for whole blocks of the field experiment were calculated and used for mass balance estimations. Compared to the average EC and CEC values of ABM-I, only very few ABM-II blocks showed an increase in exchangeable $Na^+_{(av.\ 2-8\ cm)}$ and $Mg^{2+}_{(av.\ 2-8\ cm)}$ values. The Na^+ and Mg^{2+} values were

https://doi.org/10.1346/CCMN.2017.064052 Published online by Cambridge University Press

discussed together because both decreased in a more or less similar way. The $Na^{+}_{(REF)}$ ($Mg^{2+}_{(REF)}$) concentrations in the bentonite REF materials had to be very low to allow gains in exchangeable $Na^{+}_{(REF)}$ ($Mg^{2+}_{(REF)}$): <5% (<10%). Bentonites with larger $Na^{+}_{(REF)}$ ($Mg^{2+}_{(REF)}$) values lost $Na^{+}_{(av.\ 2-8\ cm)}$ ($Mg^{2+}_{(av.\ 2-8\ cm)}$). In ABM-I, this threshold range was at much higher Na^{+} (Mg^{2+}) values. The Febex (block 9 in ABM-I) had, for example, 27% $Na^{+}_{(REF)}$ (37% $Mg^{2+}_{(REF)}$) before retrieval and 42% $Na^{+}_{(av.\ 2-8\ cm)}$ (23% $Mg^{2+}_{(av.\ 2-8\ cm)}$) after retrieval. The reacted Febex (also block 9 in ABM-II) ended up with significantly lower values: 17% $Na^{+}_{(av.\ 2-8\ cm)}$ and 8% $Mg^{2+}_{(av.\ 2-8\ cm)}$. This was typical for ABM-II in comparison to ABM-I. The two sedimentary clays showed larger increases for $Na^{+}_{(av.\ 2-8\ cm)}$ ($Mg^{2+}_{(av.\ 2-8\ cm)}$) in ABM-II in comparison to ABM-I, which was a relative effect because these samples had very low CECs in comparison to the bentonites. Average $Ca^{2+}_{(av.\ 2-8\ cm)}$ values of the reacted bentonites in ABM-II varied from 64−148%, which is much larger than in ABM-I (28−65%). Although many Ca^{2+} values in ABM-II were inflated, this increase was often an actual increase as, for example, in Febex (block 9 in ABM-I and ABM-II), which was free of soluble Ca-sulfates. While the $Ca^{2+}_{(av.\ 2-8\ cm)}$ value of reacted Febex was more or less identical in ABM-I, it increased in ABM-II from 33% to 86%. Differences between the $CEC_{(REF)}$ and the $CEC_{(av.\ 2-8\ cm)}$ values in the reacted samples in ABM-II were small with a few exceptions. The two bottom and top blocks of MX80 and the Asha 505 (block 21) in the boiling zone had a $CEC_{(av.\ 2-8\ cm)}$ decrease of up to 10 meq/100 g and one block showed a pronounced $CEC_{(av.\ 2-8\ cm)}$ increase: Rokle + 8 meq/100 g (block 7). Only 12 out of 30 samples were analyzed for CEC in ABM-I, which does not allow a comprehensive comparison of the two packages. On the other hand, many of the average $CECs_{(av.\ 1-9\ cm)}$ in the reacted samples were lower in ABM-I. The drop in average bentonite $CEC_{(av.\ 1-9\ cm)}$ (n = 9) of reacted samples was 5.5 meq/100 g (with 9 meq/100 g being the largest $CEC_{(av.\ 1-9\ cm)}$ decrease). In ABM-I, the different bentonites that lost >5 meq/100 g of the initial $CEC_{(av.\ 1-9\ cm)}$ were IBE (block 6), Febex (block 8), MX80 (block 11), Asha 505 (block 14), and Dep. CAN (block 15). The reason for this CEC decrease is not yet understood although different possible causes have been discussed. In ABM-II, the "sum-$CEC_{(av.\ 2-8\ cm)}$" values were often around 20 meq/100 g, which indicates minerals soluble in the exchange solution inflated the EC values. The parameter "sum-$CEC_{(av.\ 2-8\ cm)}$," increased strongly in the upper part close to the disintegrated blocks. In this part, halite and Ca-sulfates were detected (Kaufhold *et al*., 2017a). In ABM-I, the "sum-$CEC_{(av.\ 1-9\ cm)}$" values were <5 meq/100 g. The Na^{+}/Mg^{2+} $ratio_{(av.\ 2-8\ cm)}$ indicated differences between the upper and lower parts of the package which allowed the assumption that different zones of ion exchange equilibria occurred in ABM-II. This distribution of Na^{+}/Mg^{2+} ratios of reacted samples differed from ABM-I in which no such variation was observed. The same clays were used in ABM-I and gave a similar Na^{+}/Mg^{2+} $ratio_{(REF)}$, however, the blocks were packed in a different order which does not allow a 1:1 comparison. Comparing the average Na^{+}/Mg^{2+} $ratios_{(av.\ 1-9\ cm)}$ of the lower 15 blocks (2.9) of ABM-I with the upper 15 blocks (3.1) of ABM-I gave no significant separation of the Na^{+}/Mg^{2+} $ratios_{(av.\ 1-9\ cm)}$ in ABM-I. After 6 years, the Na^{+}/Mg^{2+} $ratio_{(av.\ 2-8\ cm)}$ was approximately in the same range for ABM-II in the lower part (3.5) as in ABM-I (in the whole package) which could be approximated as a kind of equilibrium for the ABM packages. In the upper part, the large variation in the Na^{+}/Mg^{2+}-$ratio_{(av.\ 2-8\ cm)}$ (5−10) must be explained by an additional process.

Conceptual model for water uptake from start until boiling

During operation of the experiment, water pressure dropped. If the pressure drops at such high temperatures (maximum 140ºC), the water could start boiling. Note that the maximum temperature was recorded with sensors close to the heater, whereas the temperature in the sand filter between the blocks and the rock was much lower. The design of the heaters in the ABM experiment created two temperature maxima in each of the packages. The temperature maxima were located at 1/3 and 2/3 heights in the package, which is around blocks 10 and 20 (compare to Dohrmann *et al.*, 2013b). The resulting temperature gradients became more diffuse towards the rock side, however, the temperature gradients could still be located in these blocks.

In order to maintain the pressure well above boiling, additional water was added using the artificial watering system. Results for the reacted samples of the ABM-II package obviously indicated that this technical procedure for the addition of water was not fully successful. The main observations can be summarized as follows: (1) Horizontal changes were detected; (2) the $EC_{population\ (av.\ 2-8\ cm)}$ of the blocks was not in equilibrium, although the reaction time was longer than in ABM-II; (3) the Na^{+}/Mg^{2+} $ratios_{(av.\ 2-8\ cm)}$ differed in the different parts of ABM-II; (4) some blocks were disintegrated (19−20); (5) the "sum-$CEC_{(av.\ 2-8\ cm)}$" exceeded 100% largely in the disintegrated region; and (6) halite and anhydrite precipitated in the disintegrated region. All these observations can be explained by boiling during the operation of ABM-II (Figure 6). The interactions of the buffer samples with the Äspö groundwater can be assumed as follows: At t_0, the installation started and the blocks were allowed to saturate with water without being heated. The large blue (gray in grayscale) arrow on the left (Figure 6) represents groundwater entering the buffer from the crystalline rock, whereas the small arrows at the rock/buffer boundary represent the artificial water saturation system (12 holes in total at

https://doi.org/10.1346/CCMN.2017.064052 Published online by Cambridge University Press

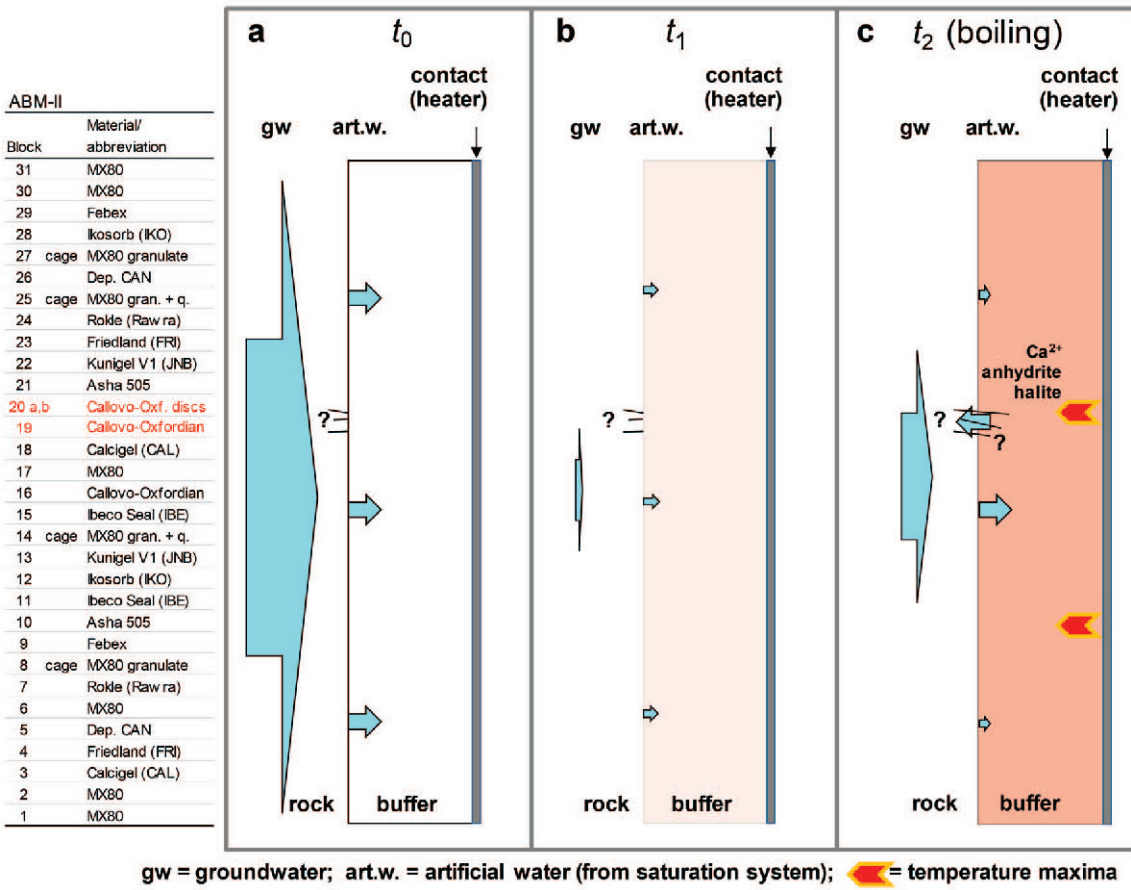

Figure 6. Conceptual model for the uptake of water from the start until boiling in ABM-II: t_0 = time of start after installation with no heating and a strong contrast between $EC_{population}$ values; t_1 = time after water saturation after heating was started and after the $EC_{population}$ has rearranged; and t_2 = the time after the peak temperature occurred, a pressure drop, the uptake of water, possible boiling, evaporation, disintegration, and additional rearrangements of the $EC_{population}$ in the boiling zone. SKB (2014) described the rock surrounding ABM-II as highly fractured.

three depths in ABM-II). In the initial phase t_0, most blocks had very different $EC_{populations}$ and started to be modified by cation exchange. At t_1, the buffer was assumed to be water saturated and the heaters were switched on. During heating, an intense rearrangement of the $EC_{population}$ occurred similar to that in ABM-I. The arrows are much smaller in this phase and represent less water uptake. As the t_2 peak temperature was reached and the pressure suddenly dropped, did this indicate a loss of water that had possibly moved towards the rock *via* fractures? The addition of water in order to avoid boiling was clearly not successful. Water from the artificial watering system plus water from the rock may have entered the buffers, although the buffers were previously water saturated. This could be explained by a water loss *via* fractures at the rock/buffer boundary. The SKB (2014) described the rock surrounding ABM-II as highly fractured. This may have caused the release of water, evaporation, disintegration, and additional re-arrangements of the $EC_{population}$ in the boiling zone. In this period, Na, Ca, and Cl rich water was entrapped and was possibly evaporated, which resulted in the observed differences in the $EC_{population}$.

CONCLUSIONS

Ion exchange reactions proceeded much faster in the buffer materials than the mineral alteration reactions which made these studies effective tools to follow the early reactions in the bentonite buffer experiments. The most significant change observed in the bentonites of the ABM-I test after the heating period was the equilibration of the $EC_{population}$ with the surrounding water and the surrounding water was assumed to have been a mixture of groundwater and water in the bentonite (Dohrmann *et al*., 2013b; Wallis *et al*., 2016). In ABM-II, the ion exchange was even more pronounced because the heating phase was 3–4 years in comparison to only about 1 year in ABM-I. The $EC_{population}$ equilibrium, however, was possibly disturbed during the experiment. In ABM-II, the cation exchange caused by the uptake of groundwater to saturate the blocks was different in

https://doi.org/10.1346/CCMN.2017.064052 Published online by Cambridge University Press

different parts of the package. The most useful parameter to distinguish between ion exchange equilibrium and boiling was the Na^{+}/Mg^{2+} ratio$_{(av.\ 2-8\ cm)}$. This parameter indicated differences between the upper and lower parts of the package. The ABM-II was first allowed to saturate with water for approximately 2–3 years. The observed differences, however, could not be explained by either the saturation before heating or the longer heating phase. The large Na^{+}/Mg^{2+} ratio-$s_{(av.\ 2-8\ cm)}$ in the upper part could possibly be explained by water loss caused by a pressure drop and water boiling and by the subsequent addition of water *via* the artificial water saturation system. The ABM-II was operated at a temperature above 100ºC, which is well above the temperature of the KBS-3 concept. The observed water loss along with a pressure drop indicated a possible risk if temperatures above 100ºC are planned to be used in concepts for the disposal of highly radioactive waste in crystalline rock. The standard conditions in the KBS-3, therefore, were reasonably set to 90ºC.

ACKNOWLEDGMENTS

The authors are grateful to Natascha Schleuning and Mirija Bardenhagen for their great analytical work. SKB is acknowledged for supplying sample material. Comments and suggestions by four anonymous reviewers and the associate editor were valuable and helped to improve the manuscript.

REFERENCES

Balmer, S., Kaufhold S., and Dohrmann, R. (2017) Cement-bentonite-iron interactions on small scale tests for testing performance of bentonites as a barrier in high-level radioactive waste repository concepts. *Applied Clay Science*, **135**, 427–436.

Bourg, I.C., Sposito, G., and Bourg, A.C.M. (2006) Tracer diffusion in compacted, water-saturated bentonite. *Clays and Clay Minerals*, **54**, 363–374.

Dixon, D.A., Martino, J.B., Vigna, l.B., Masumoto, K., and Fujita T. (2007) Overview of the evolution, performance and state of a bentonite-based tunnel seal after 5 years of operation. *Physics and Chemistry of the Earth*, **32**, 741–752.

Dohrmann, R. (2006) Cation Exchange Capacity Methodology III: Correct exchangeable calcium determination of calcareous clays using a new silver-thiourea method. *Applied Clay Science*, **34**, 47–57.

Dohrmann, R., Genske, D., Karnland, O., Kaufhold, S., Kiviranta, L., Olsson, S., Plötze, M., Sandén, T., Sellin, P., Svensson, D., and Valter, M. (2012a) Interlaboratory exchange of CEC and exchangeable cation results of bentonite buffer material. I. Cu(II)-triethylenetetramine method. *Clays and Clay Minerals*, **60**, 162–175.

Dohrmann, R., Genske, D., Karnland, O., Kaufhold, S., Kiviranta, L., Olsson, S., Plötze, M., Sandén, T., Sellin, P., Svensson, D., and Valter, M. (2012b) Interlaboratory exchange of CEC and exchangeable cation results of bentonite buffer material. II. Alternative methods. *Clays and Clay Minerals*, **60**, 176–185.

Dohrmann, R. and Kaufhold, S. (2009) Three new, quick CEC methods for determining the amounts of exchangeable calcium cations in calcareous clays. *Clays and Clay Minerals*, **57**, 338–352.

Dohrmann, R. and Kaufhold, S. (2010) Determination of exchangeable calcium of calcareous and gypsiferous bentonites. *Clays and Clay Minerals*, **58**, 513–522.

Dohrmann, R., Kaufhold, S., and Lundqvist, B. (2013a.) The role of clays for safe storage of nuclear waste. Pp. 677–710 in: *Handbook of Clay Science, Techniques and Applications* (F. Bergaya and G. Lagaly, editors). Developments in Clay Science, Vol. **5B**, Elsevier, Amsterdam.

Dohrmann, R., Olsson, S., Kaufhold, S., and Sellin, P. (2013b) Mineralogical investigations of the first package of the alternative buffer material test – II. Exchangeable cation population rearrangement. *Clay Minerals*, **48**, 215–233.

Dohrmann, R. and Kaufhold, S. (2014) Cation exchange and mineral reactions observed in MX 80 buffers samples of the prototype repository *in situ* experiment in Äspö, Sweden. *Clays and Clay Minerals*, **62**, 357–373.

Elert, K., Pardo, E.S., and Rodriguez-Navarro, C. (2015) Mineralogical evolution of di- and trioctahedral smectites in highly alkaline environments. *Clays and Clay Minerals*, **63**, 414–431.

Eng, A., Nilsson, U., and Svensson, D. (2007) Äspö Hard Rock Laboratory, Alternative Buffer Material Installation report IPR-07-15, 67 p., http://skb.se/upload/publications/pdf/ipr-07-15.pdf

Ferrage, E. (2016) Investigation of the interlayer organization of water and ions in smectite from the combined use of diffraction experiments and molecular simulations. A review of methodology, applications, and perspectives. *Clays and Clay Minerals*, **64**, 348–373.

Fröhlich, D.R. (2015) Sorption of neptunium on clays and clay minerals – A review. *Clays and Clay Minerals*, **63**, 262–276.

Gómez-Espina, R. and Villar, M.V. (2016) Time evolution of MX-80 bentonite geochemistry under thermo-hydraulic gradients. *Clay Minerals*, **51**, 145–160.

Grolimund, D., Wersin, P., Brendlé, J., Huve, J., Kiviranta, L., and Snellman, M. (2016) Interaction of titanium with smectite within the scope of a spent fuel repository: A spectroscopic approach. *Clay Minerals*, **51**, 249–266.

Holmboe, M. and Bourg, I.C. (2013) Molecular dynamics simulations of water and sodium diffusion in smectite interlayer nanopores as a function of pore size and temperature. *The Journal of Physical Chemistry C*, **118**, 1001–1013.

Holmboe, M., Wold, S., and Jonsson, M. (2010) Colloid diffusion in compacted bentonite: microstructural constraints. *Clays and Clay Minerals*, **58**, 532–541.

Ishidera, T., Kurosawa, S., Hayashi, M., Uchikoshi, K., and Beppu, H. (2016) Diffusion and retention behaviour of Cs in illite-added compacted montmorillonite. *Clay Minerals*, **51**, 161–172.

Johannesson, L.-E., Börgesson, L., Goudarzi, R., Sandén, T., Gunnarsson, D., and Svemar, C. (2007) Prototype repository: A full-scale experiment at Äspö HRL. *Physics and Chemistry of the Earth*, **32**, 58–76.

Karnland, O., Olsson, S., and Nilsson, U. (2006) *Mineralogy and Sealing Properties of Various Bentonites and Smectite-rich Clay Materials*. SKB technical report, TR 06-30.

Kaufhold, S. and Dohrmann, R. (2008) Detachment of colloids from bentonites in water. *Applied Clay Science*, **39**, 50–59.

Kaufhold, S. and Dohrmann, R. (2016) Assessment of parameters to distinguish suitable from less suitable high-level-radioactive waste bentonites. *Clay Minerals*, **51**, 289–302.

Kaufhold, S., Dohrmann, R., Koch, D., and Houben, G. (2008) The pH of aqueous bentonite suspensions. *Clays and Clay Minerals*, **56**, 338–343.

Kaufhold, S., Dohrmann, R., Sandén, T., Sellin, P., and

Svensson, D. (2013). Mineralogical investigations of the alternative buffer material test – I. Alteration of bentonites. *Clay Minerals*, **48**, 199–213.

Kaufhold, S., Dohrmann, R., and Ufer, K. (2016) Interaction of magnesium cations with dioctahedral smectites under HLRW repository conditions. *Clays and Clay Minerals*, **64**, 743-752.

Kaufhold S., Dohrmann, R., Götze, N., and Svensson, D. (2017a). Characterization of the second parcel of the alternative buffer material (ABM) experiment – I mineralogical reactions. *Clays and Clay Minerals*, **65**, 27–41.

Kaufhold, S. Dohrmann, R., and Gröger-Trampe, J. (2017b) Reaction of native copper in contact with pyrite and bentonite in anaerobic water at elevated temperature. *Corrosion Engineering, Science and Technology*, doi: 10.1080/1478422X.2017.1292201

Kaufhold, S., Sanders, D., Hassel, A.-W., and Dohrmann, R. (2015) Corrosion of high-level radioactive waste iron-canisters in contact with bentonite. *Journal of Hazardous Materials*, **285**, 464–473.

Kaufhold S., Stucki, J.W., Finck, N., Steininger, R., Zimina, A., Dohrmann, R., Ufer, K., Pentrák, M., and Pentráková, L. (2017c). Tetrahedral charge and Fe-content in dioctahedral smectites. *Clay Minerals*, **52**, 51–65.

Keller, L.M., Seiphoori, A., Gasser, P., Lucas, F., Holzer, L., and Ferrari, A. (2014) The pore structure of compacted and partly saturated MX-80 bentonite at different dry densities. *Clays and Clay Minerals*, **62**, 174–187.

Kerisit, S., Okumura, M., Rosso, K., and Mashida, M. (2016) Molecular simulation of cesium adsorption at the basal surface of phyllosilicate minerals. *Clays and Clay Minerals*, **64**, 389–400.

Klika, Z., Seidlerová, J., Valášková, M., Kliková, C., and Kolomazník, I. (2016) Uptake of Ce(III) and Ce(IV) on montmorillonite. *Applied Clay Science*, **132-133**, 41–49.

Kosec, T., Qin, Z., Chen, J., Legat, A., and Shoesmith, D.W. (2015) Copper corrosion in bentonite/saline groundwater solution: Effects of solution and bentonite chemistry. *Corrosion Science*, **90**, 248–258.

Kumpulainen, S. and Kiviranta, L. (2011) Mineralogical, chemical and physical study of potential buffer and backfill materials from ABM test package 1. Posiva Working Report 2011–41. Posiva Oy, Olkiluoto, Finland. Available online at: http://www.iaea.org/inis/collection/NCLCollectionStore/_Public/43/068/43068661.pdf.

Kumpulainen, S., Kiviranta, L., and Korkeakoski, P. (2016) Long-term effects of Fe-heater and Äspö groundwater on smectite clays – Chemical and hydromechanical results from *in situ* alternative buffer material (ABM) test package 2. *Clay Minerals*, **51**, 129–144.

Mayordomo, N., Degueldre, C. Alonso, U., and Missana, T. (2016) Size distribution of FEBEX bentonite colloids upon fast disaggregation in low ionic strength water. *Clay Minerals*, **51**, 213–222.

Meier, L.P. and Kahr, G. (1999) Determination of the cation exchange capacity (CEC) of clay minerals using the complexes of copper (II) ion with triethylenetetramine and tetraethylenepentamine. *Clays and Clay Minerals*, **47**, 386–388.

Missana, T., Alonso, U., Albarran, N., García-Gutiérrez, M., and Cormenzana, J.-L. (2011) Analysis of colloids erosion from the bentonite barrier of a high level radioactive waste repository and implications in safety assessment. *Physics and Chemistry of the Earth, Parts A/B/C*, **36**, 1607–1615.

Olsson, S. and Karnland, O. (2011) Mineralogical and chemical characteristics of the bentonite in the A2 test parcel of the LOT field experiments at Äspö HRL, Sweden. *Physics and Chemistry of the Earth*, **36**, 1545–1553.

Peng, Y., Zhang, H., Yang, B., Wang, X., Shao, X., and Liu, P. (2016) Ice-bentonite powder mixing method to improve the homogeneity of compacted bentonite in an initial sample preparation stage. *Clays and Clay Minerals*, **64**, 706-718.

Plötze, M., Kahr, G., Dohrmann, R., and Weber, H. (2007) Hydro-mechanical, geochemical and mineralogical characteristics of the bentonite buffer in a heater experiment. The HE-B project at the Mont Terri rock laboratory. *Physics and Chemistry of the Earth*, **32**, 730–740.

Rivard, C., Pelletier, M., Michau, N., Razafitianamaharavo, A., Abdelmoula, M., Ghanbaja, J., and Villiéras, F. (2016) Reactivity of Callovo-Oxfordian claystone and its clay fraction with metallic iron: Role of non-clay minerals in the interaction mechanism. *Clays and Clay Minerals*, **63**, 290–310.

Samper, J., Naves, A., Montenegro, L., and Mon, A. (2016) Reactive transport modelling of the long-term interactions of corrosion products and compacted bentonite in a HLW repository in granite: Uncertainties and relevance for performance assessment. *Applied Geochemistry*, **67**, 42–51.

Sasamoto, H., Isogai, B., Kikuchi, H., Satoh, H., and Svensson, D. (2017) Mineralogical, physical and chemical investigation of compacted Kunigel V1 bentonite in contact with a steel heater in the ABM test package 1 experiment, Äspö laboratory, Sweden. *Clay Minerals*, **52**, 127–141.

Sellin, P. and Leupin, O. (2014) The use of clay as an engineered barrier in radioactive waste management – a review. *Clays and Clay Minerals*, **61**, 477–498.

SKB (2007) RD&D Programme 2007. Programme for research, development and demonstration of methods for the management and disposal of nuclear waste. TR-07-12, Swedish Nuclear Fuel and Waste Management Company (SKB), Stockholm, Sweden. http://www.skb.se/upload/publications/pdf/TR-07-12_FUD_2007_eng_webb.pdf.

SKB (2014) Äspö Hard Rock Laboratory, Annual Report 2013. TR-14-17, Swedish Nuclear Fuel and Waste Management Company (SKB), Stockholm, Sweden. http://www.skb.com/publication/2720398/TR-14-17.pdf.

Stanjek, H. and Künkel, D. (2016) CEC determination with Cu-triethylenetetramine: recommendations for improving reproducibility and accuracy. *Clay Minerals*, **51**, 1–17.

Svensson D., Dueck A., Nilsson U., Olsson S., Sandén T., Lydmark S., Jägerwall S., Pedersen K., and Hansen S. (2011) *Alternative Buffer Material. Status of the Ongoing Laboratory Investigation of Reference Materials and Test Package 1*. TR-11-06. Svensk Kärnbränslehantering AB (SKB), Stockholm, Sweden. http://skb.se/upload/publications/pdf/TR-11-06.pdf.

Szakálos, P. and Seetharaman, S. (2012) *Corrosion of Copper. Technical Note 2012:17*. Report number: 2012:17 ISSN: 2000-0456.

Tournassat, C., Bourg, I., Holmboe, M., Sposito, G., and Steefel, C.I. (2016) Molecular dynamics simulations of anion exclusion in clay interlayer nanopores. *Clays and Clay Minerals*, **64**, 74–388.

van Geet, M. and Dohrmann, R. (2016) Overview of the clay mineralogy studies presented at the 'Clays in natural and engineered barriers for radioactive waste confinement' meeting, Brussels, March 2015. *Clay Minerals*, **51**, 125–128.

Wallis, I., Idiart, A., Dohrmann, R., and Post, V. (2016) Reactive transport modelling of groundwater-bentonite interaction: effects on exchangeable cations in an alternative buffer material *in-situ* test. *Applied Geochemistry*, **73**, 59–69.

Wersin, P. and Birgersson, M. (2014) Reactive transport modelling of iron–bentonite interaction within the KBS-3H disposal concept: the Olkiluoto site as a case study. in: *Geological Society, London, Special Publications 2014*, vol. 400, pp. 237–250.doi:10.1144/SP400.24.

Wersin, P., Jenni, A., and Mäder, U.K. (2015) Interaction of corroding iron with bentonite in the ABM1 Experiment at Äspö, Sweden: A microscopic approach. *Clays and Clay Minerals*, **63**, 51–58.

(*Received 26 October 2016; revised 11 April 2017; Ms. 1145; AE: M. Plötze*)